Journal of Power Sources 236 (2013) 10–16

Contents lists available at SciVerse ScienceDirect

Journal of Power Sources

journal homepage: www.elsevier.com/locate/jpowsour

Surfactant-assisted nanocrystal filling of TiO_2 nanotube arrays for dye-sensitized solar cells with improved performance

Zuobao Yang [a,c], Dengyu Pan [a,b,*], Chen Xi [b], Jinghui Li [b], Jianwei Shi [a], Fei Xu [a], Zhongquan Ma [a,**]

[a] SHU-SolarE R&D Lab, Department of Physics, Shanghai University, Shanghai 200444, PR China
[b] Institute of Nanochemistry and Nanobiology, Shanghai University, Shanghai 200444, PR China
[c] Department of New Energy Science and Engineering, Xinyu University, Xinyu 338004, PR China

HIGHLIGHTS

- We report a novel surfactant-assisted vacuum impregnation approach.
- Debris-free and highly ordered TiO_2 nanotube arrays were prepared.
- A controllable TiO_2 nanocrystal/nanotube composite electrode was prepared.
- The composite electrode exhibits enhanced light-harvesting and dye adsorbing capacities.
- The efficiency of DSSCs was significantly improved with the composite electrode.

ARTICLE INFO

Article history:
Received 12 October 2012
Received in revised form
11 February 2013
Accepted 13 February 2013
Available online 28 February 2013

Keywords:
Titanium oxide
Nanotube arrays
Nanocrystal
Surfactant
Dye-sensitized solar cells

ABSTRACT

Uniform, debris-free, fewer-crack, and highly ordered TiO_2 nanotube arrays are prepared by a two-step anodic oxidation method, and a surfactant-assisted vacuum impregnation approach is developed to control the incorporation of sub-10-nm TiO_2 nanocrystals into the nanotube arrays. By using the double polymer surfactants of polyethylene glycol and Polyvinyl Pyrrolidone as a sacrificed template, nanocrystal over-agglomeration is prohibited, and thin nanocrystal mesoporous layers are formed on both inner and outer nanotube walls. The application of the nanocrystal filled nanotube arrays as the photoanode for dye-sensitized solar cells has been evaluated. The incorporation of the nanocrystals into the nanotube arrays is found to enhance dye absorption and light-harvesting capacities markedly. As a result, the solar cells based on the filled nanotube arrays hold a short-circuit current density 2.06 times and a power-conversion efficiency 1.94 times higher than those based on the unfilled nanotube arrays.

1. Introduction

Dye-sensitized solar cells (DSSCs) have attracted increasing attention as a promising alternative to conventional high-cost silicon solar cells [1–5]. Apart from the low-cost fabrication, high power-conversion efficiency (PCE) up to 12% achieved so far [6] is also alluring. The photoelectrochemical cells operate involving nearly concomitant electron and hole injection from a photoexcited dye into a semiconductor photoanode, typically composed of porous TiO_2, and a redox electrolyte, commonly consisting of I^-/I_3^- redox couple, respectively. Being loaded with both the dye and the electrolyte, thus playing crucial roles in highly efficient solar light harvesting and electron–hole separation/transfer, the photoanode is conventionally constructed into a mesoporous nanocrystal (NC) film with a large enough internal surface area for maximizing monolayer dye absorption and facilitating redox penetration at a given film thickness [7]. This disordered photoanode architecture, however, is subjected to a short electron diffusion length of 7–30 μm [8–10] on account of random electron walk [11,12], which leads to the limit of the active film thickness below 10 μm to guarantee efficient transport of photoinjected electrons to the outer circuit. The insufficient film thickness will, in turn, result in substantial solar light loss ascribed to low light trapping capability. To collect the lost part of the incident solar light, it is needed to construct an additional reflection layer composed of larger NCs on the active layer [13].

* Corresponding author. SHU-SolarE R&D Lab, Department of Physics, Shanghai University, Shanghai 200444, PR China. Tel.: +86 21 66135276 106; fax: +86 21 66135275.
** Corresponding author.
E-mail addresses: dypan617@shu.edu.cn (D. Pan), zqma@shu.edu.cn (Z. Ma).

0378-7753/$ – see front matter © 2013 Elsevier B.V. All rights reserved.
http://dx.doi.org/10.1016/j.jpowsour.2013.02.037

On the other hand, one-dimensional (1D) nanostructures have been used to produce 1D photoanodes [14–16], which may provide a more effective pathway for electron transport [17,18] and less ohmic loss [8,19] than the NC photoanodes. In this regard, self-organized, vertically oriented TiO_2 nanotube arrays (NTAs) as the photoanode is especially attractive [20], because the tube walls provide a vertical pathway for electron transport to the collection electrode. Recent experiments have shown that the electron diffusion lengths of NTAs are on the order of 100 μm [21], which allows NTA films to be made longer for enhancing light trapping ability. Despite these advantages, NTA-based DSSCs were found to show very low current densities and thus low PCE [18,22]. The low current densities are usually ascribed to the sunlight loss due to undesirable solar absorption by the counter electrode and the electrolyte under the back illumination mode, in particular, to the smooth nanotube walls responsible for insufficient internal surface area for dye loading. To address the two issues, some strategies have been developed. To overcome the first issue, the transfer of grown NTA films from the Ti substrate to transparent conducting oxides (TCOs) [23,24] and direct growth of NTA films on TCOs [25] have been reported for allowing more efficient front illumination modes to be used. For the second issue, the fabrication of hierarchical nanostructure photoanodes has been extensively investigated, involving the surface modification of NTAs with sub-10-nm TiO_2 NCs with a higher specific surface area by post-growth [26–34] or post-assembly [35–40] routes. Because of the incorporation of TiO_2 NCs into the arrays, the roughness factor or internal surface area of the composites markedly increases compared with NTAs alone, and hence, the overall performance of the composite photoanodes is substantially improved. In this configuration, vertically oriented TiO_2 nanotubes themselves function mostly as a highway for electron transport or as a three-dimensional extension of the collection electrode, while individual TiO_2 NCs deposited on the nanotube walls serve as a sub-10-nm substrate for dye absorption. To maximize the dye absorption and simultaneously minimize the interfacial area between adjacent TiO_2 NCs for achieving the optimized overall performance of the photoanodes, uniform and dense TiO_2 NCs should be well dispersed on the whole inner and outer surfaces of NTAs. Nowadays, it remains challenging to control the ideal deposition of TiO_2 NCs for currently developed deposition methods. In many cases, TiO_2 NCs densely pile up, and consequently, the overall surface area of NCs is substantially reduced. In particular, NCs over-agglomerate into thick and dense blocks at the entrance of the nanotubes, where serious blockage occurs.

Herein, we report for the first time a simple surfactant-assisted vacuum impregnation (SVI) approach for the controlled assembly of sub-10-nm TiO_2 NCs into NTAs as a more efficient photoanode for DSSCs. Double polymer surfactants were introduced to guide the NC assembly process and prohibit the NCs from over-agglomeration. Through the double-layer isolation by the long-chain organic molecules, we are capable of achieving well-dispersed NC deposition on the nanotube walls. The effects of the NC filling on visible-light reflection, dye absorption and performances of the NTA-based DSSCs were explored.

2. Experimental

2.1. Preparation of TiO_2 NTAs

TiO_2 NTAs were prepared by twice potentiostatic anodizations in a two-electrode electrochemical cell. Prior to the first anodic oxidation, Ti foils (250 μm in thickness, 99.7% in purity, Sigma Aldrich) were degreased by ultrasonication in acetone, ethanol and deionized (DI) water successively before drying with nitrogen. The dried Ti foils were immersed into a mixture of hydrofluoric acid (HF), nitric acid (HNO_3) and DI water (HF:HNO_3:DI = 1:4:5, v/v) for 30 s to smoothen the surface. Rinsed with DI water and blow-dried with a nitrogen gun, the foils were anodically oxidized in ethylene glycol containing 0.4 wt% NH_4F and 2 vol% H_2O for 2 h at room temperature by applying 50 V DC potential. The as-grown NTA films were rinsed with DI water for several times, which allowed the first-grown uneven films to be removed by a strong nitrogen stream. Flat TiO_2 NTA films were then grown by second anodization in the same electrolyte. Finally, the NTA films were calcined in air at 450 °C for 2 h with a heating rate of 1 °C min^{-1}.

2.2. Synthesis of PEG-coated TiO_2 NCs

PEG-coated TiO_2 NCs were synthesized by a hydrothermal route as described elsewhere [41]. Typically, prior to adding 1 mL concentrated hydrochloric acid (37%) drop by drop with a micro-pipette, 3 mL of tetra-*n*-butyl titanate ($(C_4H_9O)_4Ti$, 98%) and 6 mL of polyethylene glycol (PEG, PEG-400) were mixed under magnetic stirring to form a titanium alkoxide complex. The precursor was then transferred to a teflon autoclave for hydrothermal reaction at 150 °C for 10 h in a dry oven. Separated by high-speed (12,000 rpm) centrifugation, the precipitates were washed with ethanol and dried at 60 °C overnight. Finally, it was grinded into powder, which was highly water-soluble due to the PEG-coating.

2.3. Surfactant-assisted NC filling of NTAs

The filling of the flat NTAs with the water-soluble PEG-coated TiO_2 NCs was performed by the SVI approach in the presence of Polyvinyl Pyrrolidone (PVP, PVP-K30). Typically, PEG-capped TiO_2 NCs was dispersed in 10 mL aqueous solution of PVP. Then the mixed solution was subsequently treated ultrasonically for 30 min to form a stable and homogenous NC dispersion. The TiO_2 NTAs were filled with the NC dispersion under the vacuum of −0.1 MPa and were annealed at 500 °C for 30 min in air to remove the two surfactants of PVP and PEG. Two NC-filled NTA samples with increasing filling levels, denoted by NC-NTA-1 and NC-NTA-2, were obtained by varying the concentrations of the NCs and PVP (300 mg NCs and 0.38 M PVP for NC-NTA-1, 600 mg NCs and 0.76 M PVP for NC-NTA-2). In comparison, the as-annealed second-anodized NTA samples were denoted with unfilled-NTA hereafter.

2.4. Fabrication of DSSCs

The pristine and filled NTAs grown on Ti substrates were used as a photoanode sensitized with N719 (cis-diisothiocyanato-bis (2,2′-bipyridyl-4,4′-dicarboxylato)ruthenium(II) bis (tetrabutylammonium)). The photoanode ($\sim$0.12 cm^2) was sensitized by immersing the hot (80 °C) one into anhydrous ethanol containing 3×10^{-4} M N719 for 24 h at room temperature. The dye-loaded photoanode, a 60-μm-thick hot-melt sealed film as a spacer (DHS-SN1760, Heptachroma, Dalian, China), and an apertured counter electrode (platinized FTO glass), were assembled together with a hot-melt machine. A redox electrolyte (acetonitrile solution of DMPII/LiI/I_2/TBP/GuSCN, DHS-E23, Heptachroma, Dalian, China) was injected into the cell through the aperture in the counter electrode under vacuum conditions. Finally, the cells were enveloped with a stack layer of hot-melt sealed tablet and glass.

2.5. Characterization

The crystalline phases of NTAs and NCs were identified by X-ray diffraction (XRD, D/Max-2200pc, Rigaku, Japan). The morphology, thickness and NC filling of NTAs were characterized with a field

emission scanning electron microscope (FE-SEM, S-4800 Hitachi, Japan). The microstructure was further investigated with a high-resolution transmission electron microscope (HRTEM, JEM-2010F, JEOL, Japan). Ultraviolet–visible (UV–vis) reflectance and absorption spectroscopy of the samples were obtained with a spectrophotometer (U3010, Hitachi, Japan). The photovoltaic performance of the cells was measured using a computer-controlled keithly-2400 source meter under illumination intensity of 100 mW cm^{-2} at room temperature with a standard solar simulator. Electrochemical impedance spectroscopy (EIS) measurement was performed on an electrochemical workstation (CHI660D, CH instruments, Shanghai, China).

3. Results and discussion

Highly ordered TiO_2 NTAs are usually prepared through a one-step anodic oxidation process, which produces uneven membrane surface, cracks, and a covering of thin debris blocking nanotubes underneath, as clearly demonstrated by SEM images (inset in Fig. 1(a)). To circumvent these issues, a two-step anodic oxidation strategy was used to prepare flat and debris-free TiO_2 NTAs. This procedure included several successive sub-processes: the first anodic oxidation of a degreased and chemically polished Ti foil, the removal of the as-grown NTAs by rinsing with water and blowing with a strong N_2 stream, and the second anodic oxidation (Scheme 1(a)–(d)). The removal of the first-grown NTAs left a hexagonally packed pattern composed of regular shallow pits on the Ti foil surface (Scheme 1(c) and Fig. 1(b)). This dense pattern served as a template to guide the vertical growth of nanotubes underneath during the second oxidation, and itself evolved into a top macroporous layer without the presence of debris on it (Scheme 1(d) and Fig. 1(c)). The presence of the top template well confined the lengths of the nanotubes underneath, rendering the second-grown nanotube array more uniform, evener and smoother (Fig. 1(c)). Moreover, cracks were markedly reduced in number, likely because the uniform tube lengths can effectively buffer the stress formed during the growth and subsequent annealing processes (indeed, cracks were regularly observed in dramatically uneven areas (Fig. 1(a))). The resultant flat and debris-free TiO_2 NTAs with an average tube length of 14.5 μm (Fig. 1(d)) and an average inner diameter of 110 nm were further annealed at 450 °C to convert them from amorphous to anatase phases.

The SVI approach was used to assemble water-soluble TiO_2 NCs into the NTAs, as shown in Scheme 1(e). Specifically, highly water-soluble anatase TiO_2 NCs coated with a water-soluble polymer surfactant (PEG) were synthesized by hydrothermal route. Their average diameter, determined by the analysis of their XRD pattern (Fig. 2(b)) through the Scherrer equation, is about 8 nm, far smaller than the inner diameter of the nanotubes. Their small size and excellent water solubility allowed their aqueous dispersion to penetrate the nanotubes without hindrance when the NTAs were socked in the dispersion under vacuum-pumping. Notably, another water-soluble polymer surfactant, PVP, was also added to the NC dispersion to control the assembly and aggregation of the TiO_2 NCs within the NTAs. In the solution, long-chain PVP molecules could be coupled with the PEG molecules attached to the NC surface through the hydrogen bond interaction between OH and C=O functional groups present in PEG and PVP, thus extending the organic monolayer located at the NC surface to the thicker double layers. Meanwhile, more free PVP molecules were assemble into micelles in the solution (Scheme 1(e)). During drying, the water-soluble NCs were deposited on the inner and outer walls of the nanotubes and were assembled with the PVP micelles that well isolated the NCs. Further annealing in air removed the surfactants, leaving a mesoporous NC layer on the tube walls (Scheme 1(f)).

The typical NC filled nanotube sample, NC-NTA-2, was characterized in detail by XRD, SEM, and TEM. Fig. 2 shows the XRD pattern of the NC-NTA-2 sample, as well as those of the unfilled NTA and the TiO_2 NCs for comparison. For the NC sample, the (101), (004), (200), (105) and (204) diffraction peaks of anatase are

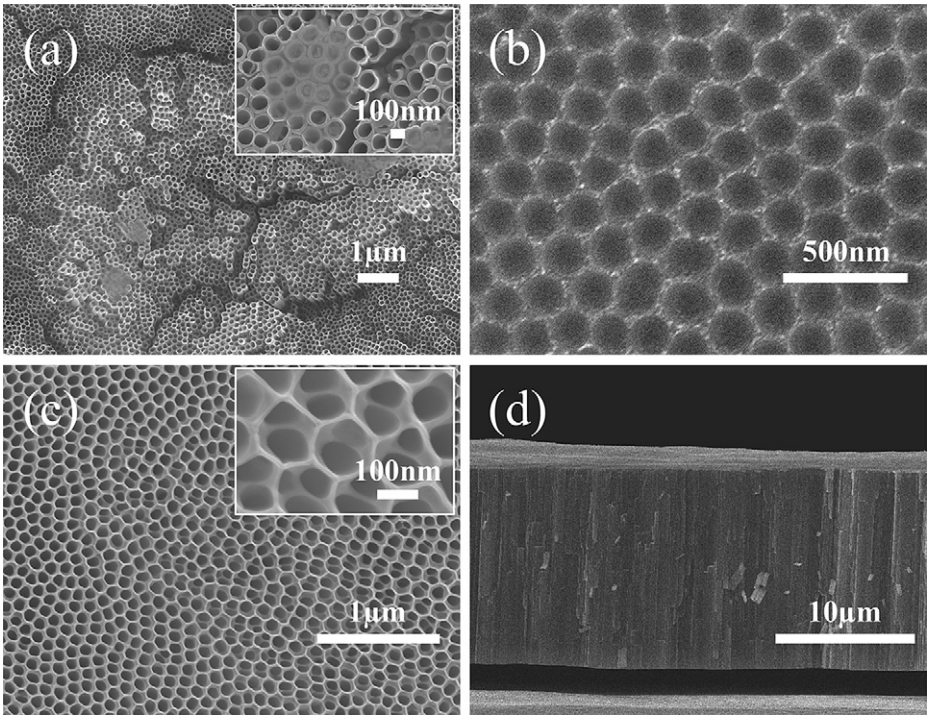

Fig. 1. SEM images of (a) top view of first-anodized TiO_2 NTA, (b) top view of the substrate after removing the NTA layer, (c) and (d) top and cross-sectional views of second-grown TiO_2 NTAs, respectively (insets show the respective magnified images).

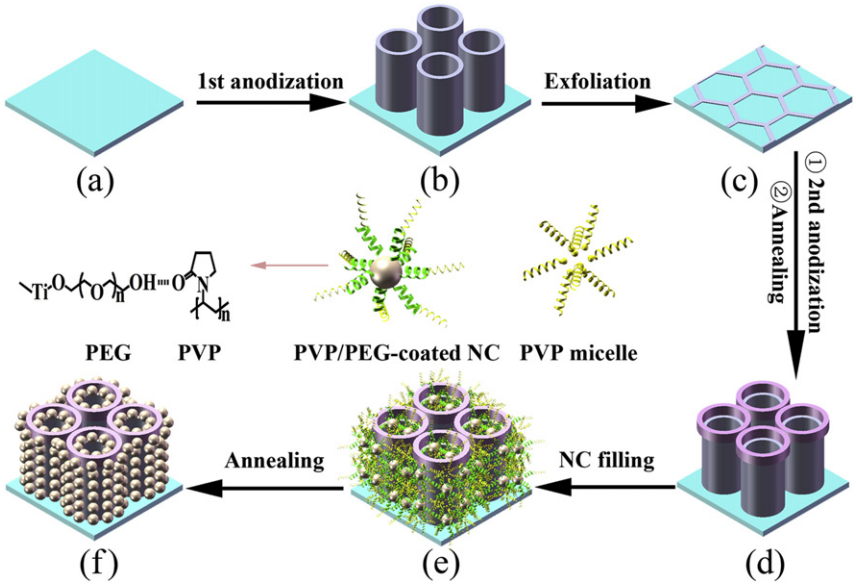

Scheme 1. Preparation (a–d) and NC filling (e–f) of flat and debris-free TiO_2 NTAs.

broadened as a consequence of their small size (<10 nm). For the unfilled NTA on the Ti substrate, relatively sharp diffraction peaks were observed. Except for the (101) and (102) peaks indexed to the Ti substrate, all other diffractions are indexed to the TiO_2 anatase phase. After the incorporation of the anatase TiO_2 NCs into the anatase NTA, no marked change in the XRD profile occurs apart from the pronounced enhancement of the (004) and (105) peaks as a result of the overlap of these peaks from the NCs and the NTA. Fig. 3 shows the SEM images of the typical NC filled NTA. On the top macroporous layer, the deposition of the NCs was not found to block the entrance of the nanotubes underneath (Fig. 3(a)), which is also confirmed by the oblique view of the upper nanotube arrays (Fig. 3(b)). On the inner nanotube walls, uniform NC layers were deposited, which is demonstrated clearly from some broken nanotube arrays (Fig. 3(c)). On the outer walls, NCs were also deposited in large quantities (Fig. 3(d)). The magnified view of the deposited NC layers (insets in Fig. 3(d)) shows that the sub-10-nm

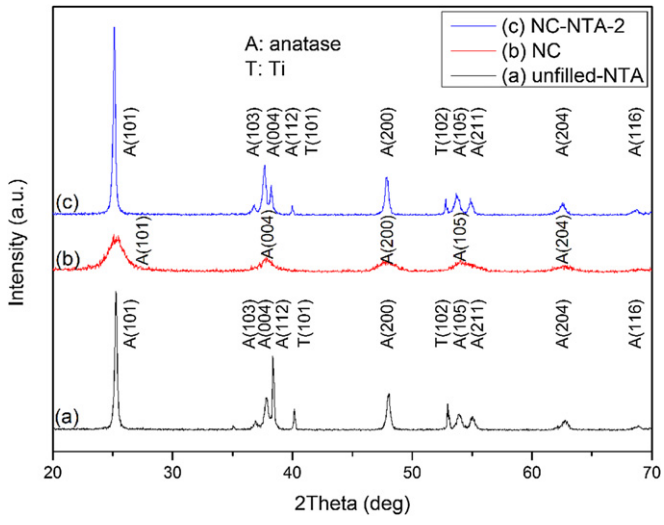

Fig. 2. XRD patterns of (a) unfilled-NTA annealed at 450 °C, (b) hydrothermally synthesized TiO_2 NCs, and (c) NC-NTA-2.

NCs were well dispersed on the tube walls, and assembled into a thin mesoporous layer. There is an obvious contrast between NC-free, smooth nanotube walls and NC-landing, coarse nanotube walls (inset in Fig. 3(d)). Some fragments scraped off NC-NTA-2 were examined by TEM (Fig. 4(a)), which also shows that NC mesoporous layers were incorporated into the arrays. The high-resolution TEM image (Fig. 4(b)) displays (101) lattice fringes of anatase TiO_2 NCs within the nanotube arrays. The selected area electron diffraction pattern (inset in Fig. 4(b)) shows diffraction dot arrays and diffraction rings of (101), (004) and (200) planes, corresponding to the nanotube wall and NC layer, respectively.

To evaluate the effects of the surfactant-assisted NC filling on the performances of DSSCs using TiO_2 NTAs as photoanodes, representative TiO_2 NTA samples with different NC filling levels (unfilled-NTA, NC-NTA-1, NC-NTA-2) were explored. The DSSCs were assembled using N719 dye as a sensitizer of the photoanodes, the I^-/I_3^- redox couple as an electrolyte, and platinized FTO glass as a counter electrode, and the performances of the cells were measured using the backside-illumination mode under simulated AM 1.5G sunlight (100 mW cm^{-2}). The photocurrent–voltage (J–V) characteristics of the representative samples are shown in Fig. 5, and typical performance parameters such as open-circuit voltage (V_{oc}), short-circuit current density (J_{sc}), fill factor (FF), and PCE (η), are presented in Table 1. Notably, the NC filled NTA-based DSSCs exhibit a much higher J_{sc} than the unfilled NTA-based DSSC. For the NC-NTA-2-based DSSC with a higher NC content, the J_{sc} is 12.34 mA cm^{-2}, being 1.16 and 2.06 times as high as that of the NC-NTA-1-based DSSC with a lower filling level and the unfilled-NTA-based DSSC, respectively. Different from J_{sc}, V_{oc} nearly keeps unchanged (~0.65 V), while FF slightly decreases from 0.69 to 0.64 with increasing NC content. According to the equation, $\eta = J_{sc}V_{oc}FF/P_{in}$, where P_{in} = 100 mW cm^{-2}, the PCE values of the DSSCs based on unfilled-NTA, NC-NTA-1, NC-NTA-2 are determined to be 2.68%, 4.62%, and 5.21%. Evidently, for the DSSCs based on NC filled NTAs, the remarkable increase in J_{sc} largely contributes to their significant improvement in PCE.

To understand the effects of the NC filling on the performances of the NTA-based DSSCs, we measured the reflectance spectra of the three typical NTA films in the wavelength range of 300–900 nm prior to N719 loading (Fig. 6). As expected, all the NTA

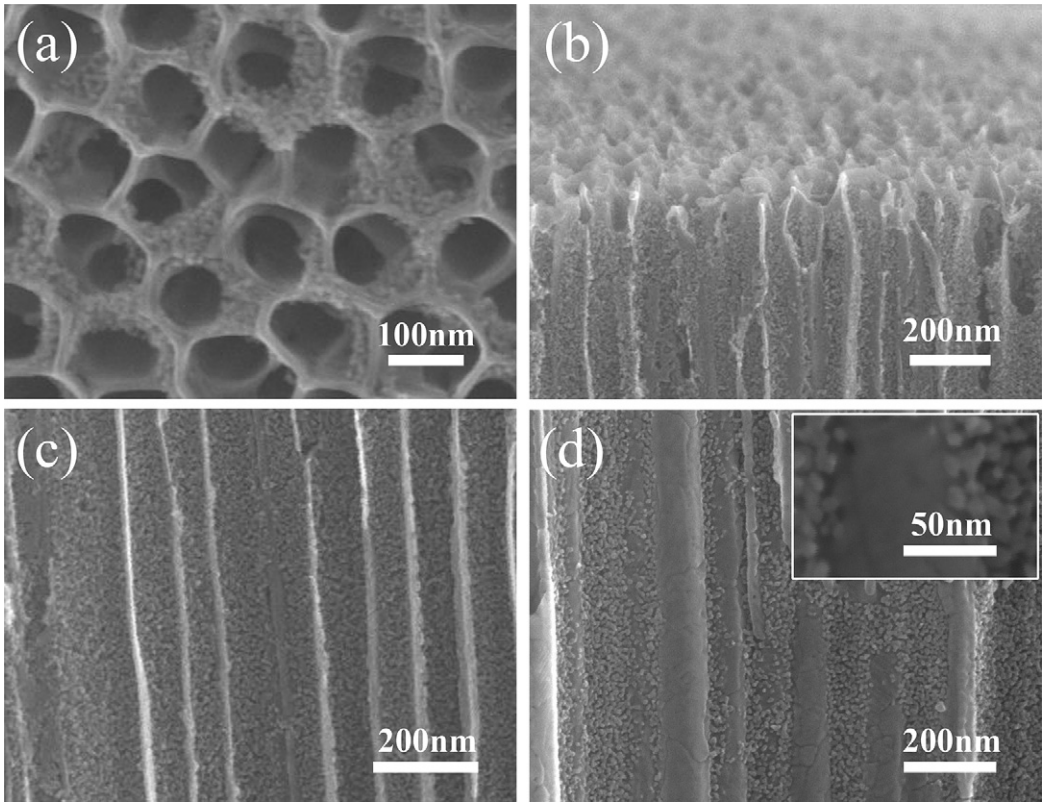

Fig. 3. SEM images of NC filled TiO_2 NTAs (NC-NTA-2): (a) top view, (b) oblique view, (c) cross-sectional view of cleaved nanotubes showing their inner walls and uniformly deposited NC mesoporous layers and (d) cross-sectional view of the outer walls of the NC filled NTAs (inset shows the magnified view of a NC mesoporous layer deposited on the outer walls).

films exhibit considerably low reflectivity from UV to visible regions (UV–vis) owing to a strong light-trapping capacity for the unique nanotube array morphology. Interestingly, remarkable decrease in reflectivity induced by NC filling was observed. For example, at 530 nm, where N719 shows a strong absorption peak, the NC-NTA-2 sample shows reflectance of 11.4%, lower than that (15.9%) of the unfilled-NTA. The reduced reflection can be ascribed to enhanced light-scattering from the nanotube walls coarsened by the deposition of NC mesoporous layers observed by SEM. Evidently, the reduced visible-light reflection boosts an ability of N719 anchored on the nanotube walls to harvest visible light. Apart from the reduced visible-light reflection, the capacity of dye loading that greatly influences solar light harvesting efficiency was also examined. Specifically, the monolayer N719 dye anchored on unfilled NTAs and filled NTAs was desorbed into a 0.1 M NaOH solution in a mixed solvent (DI/ethanol = 1:1, v/v) and the amount of N719 dye was estimated by measuring UV–vis absorption spectroscopy of the resultant solution. Dye adsorbance was determined to be 1.10×10^{-7} mol cm^{-2}, 1.87×10^{-7} mol cm^{-2} and 2.04×10^{-7} mol cm^{-2} for the unfilled-NTA, NC-NTA-1 and NC-NTA-2 samples, respectively. The dye adsorbance for NC-NTA-2 is nearly 2 times higher than that for the unfilled-NTA, 1.7 times higher for NC-NTA-1. The enhancement of the dye absorption with increasing the NCs dose is related to the formation of the unique and effective NC mesoporous layer on the nanotube wall. Thus, we can draw the conclusion that the remarkable increase in J_{sc} and PCE for the NC filled NTAs is correlated with the boosted light-harvesting capacity accorded by the incorporation of the NC

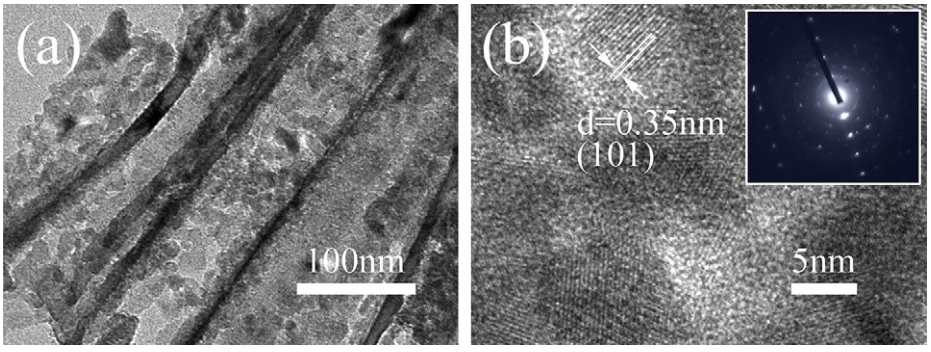

Fig. 4. Low-magnified (a) and high-resolution (b) TEM images of nanotube fragments scraped off NC-NTA-2 (inset shows the images of selected area electron diffraction).

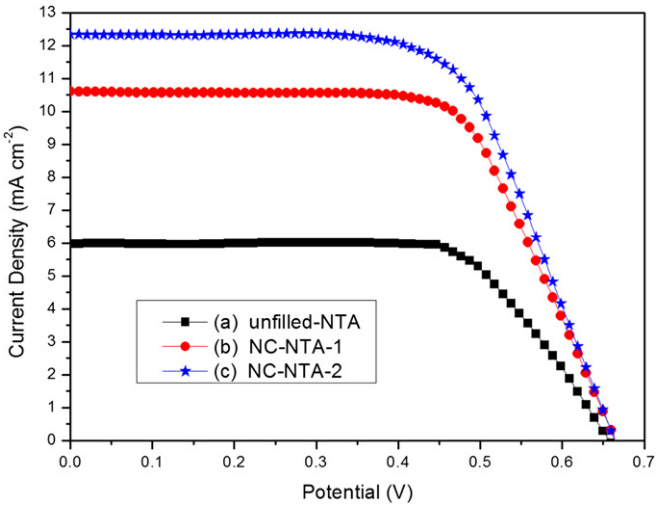

Fig. 5. Photocurrent–voltage (J–V) measurements of DSSCs based on (a) unfilled-NTA, (b) NC-NTA-1 and (c) NC-NTA-2 as photoanodes.

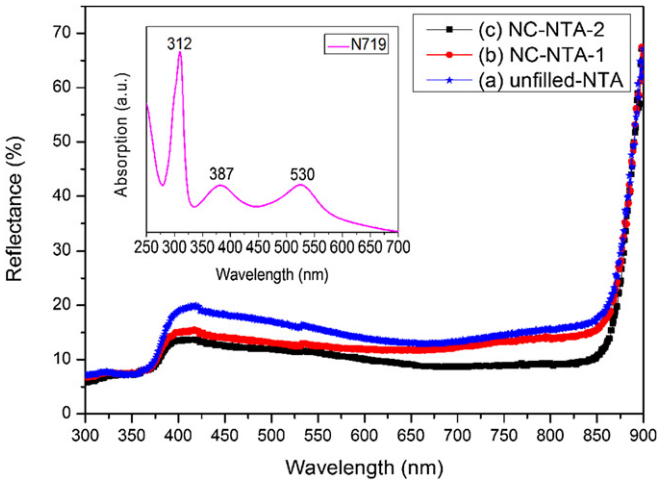

Fig. 6. Normalized reflectance spectra of (a) the unfilled-NTA and (b) NC-NTA-1 and (c) NC-NTA-2 (inset shows the UV–vis absorption spectra of N719 in ethanol).

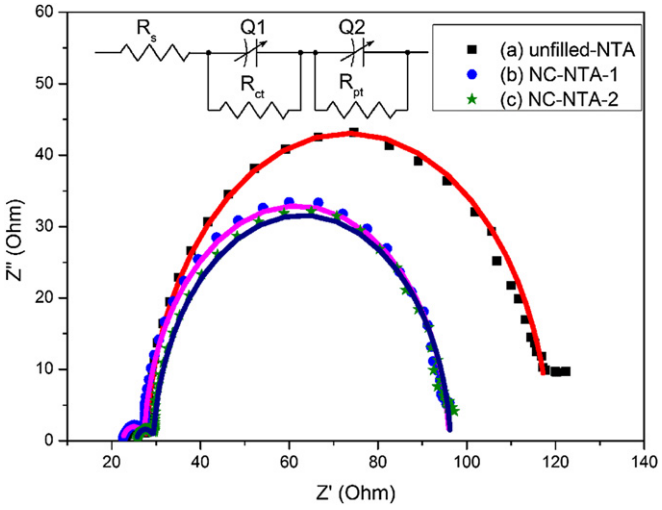

Fig. 7. The Nyquist plots of EIS of the DSSCs based on (a) unfilled-NTA, (b) NC-NTA-1, (c) NC-NTA-2 (the continuous lines corresponding to the fitting results, and the inset is the equivalent circuit for fitting the plots).

porous layers into the NTAs through the effects of reflection reduction and more dye absorbance.

EIS was further employed to study the photo-electrochemical kinetics of the NTA-based DSSCs [42,43]. The EIS measurements were performed under illumination with AM 1.5 G simulated solar light at an applied DC bias of V_{oc} in a perturbation alternative signal of 5 mV. The Nyquist plots of the obtained impedance data were depicted in Fig. 7. The measuring frequency range was from 10^{-1} Hz–10^{5} Hz. These plots are well fitted into two semicircles using the ZsimpWin software in terms of an appropriate equivalent circuit composed of constant phase elements (Q) and resistors (R) (inset in Fig. 7). The smaller semicircle at high frequency was ascribed to electron transfer at the interface of electrolyte and Pt counter electrode while the larger semicircle at medium frequency was associated with electron transport in the TiO_2 electrode and electron back reaction at the interface of the TiO_2 photoanode and the electrolyte [44–47]. Some typical electrochemical parameters derived from the fitting were summarized in Table 1, including charge transfer resistances (R_{pt}) at the Pt counter/electrolyte interface and charge transfer resistances (R_{ct}) related to photoexcited electron–hole recombination at the TiO_2/electrolyte. The values of R_{pt} is nearly identical for unfilled-NTA, NC-NTA-1 and NC-NTA-2 due to the identical commercial counter electrode using in this work while the values of R_{ct} were decreased with the increasing filled mesoporous NC content. However, the value of R_{ct} with sample unfilled-NTA is 90.9 Ω while it dramatically decreases to 68.82 Ω with sample NC-NTA-1. The R_{ct} turned to be 66.83 Ω with sample NC-NTA-2 when the NC content was further increased. The decrease of the values of R_{ct} suggested that more electrons was injected into the conduction band of TiO_2 [48,49] with more mesoporous TiO_2 NC attached on NTA, which is consistent with remarkable increase in J_{sc} of DSSCs based on NC-NTA-2.

Table 1
Photovoltaic performance parameters of DSSCs and derived parameters of EIS based on unfilled-NTA, NC-NTA-1, NC-NTA-2.

Photoanode	J_{sc} (mA cm^{-2})	V_{oc} (V)	FF	η (%)	R_{ct} (Ω)	R_{pt} (Ω)
Unfilled-NTA	5.98	0.65	0.69	2.68	90.90	4.78
NC-NTA-1	10.61	0.66	0.66	4.62	68.82	5.01
NC-NTA-2	12.34	0.66	0.64	5.21	66.83	3.94

4. Conclusions

In summary, a surfactant-assisted vacuum impregnation approach has been developed to control the incorporation of sub-10-nm TiO_2 NCs into uniform, debris-free and fewer-crack NTAs prepared by two-step anodic oxidation. By using the double polymer surfactants of PEG and PVP as a sacrificed template, NC over-agglomeration was prohibited, and thin NC mesoporous layers were formed on both inner and outer nanotube walls. The TiO_2 NC filled nanotube arrays exhibit enhanced light-harvesting and dye absorption capacities. A remarkable improvement was achieved with a power-conversion efficiency of 5.21% with back-illuminated mode under AM 1.5G, corresponding to 194% enhancement compared with DSSCs based on unfilled-NTA. We believe that the surfactant-assisted vacuum impregnation approach can be extensively employed to synthesize other hierarchical and/or composite nanostructures for a vast array of applications.

Acknowledgment

This work was partly supported by Natural Science Foundation of China (Nos. 91233102, 60876045, 11174194 and 11025526),

Innovation Program of Shanghai Municipal Education Commission (No. 13ZZ076), Shanghai Leading Basic Research Project (No. 09JC1405900), Shanghai Leading Academic Discipline Project (Nos. S30105 and S30109), R&D Foundation of SHU-SOENs PV Joint Lab (No. SS-E0700601) and Youth Science Fund Project of the Education Department of Jiangxi Province (No. GJJ10276). Some of the measurements were performed in Instrumental Analysis and Research Center of Shanghai University of China.

References

[1] B. O'Regan, M. Gratzel, Nature 353 (1991) 737–740.
[2] M. Gratzel, Nature 414 (2001) 338–344.
[3] A. Hagfeldt, G. Boschloo, L. Sun, L. Kloo, H. Pettersson, Chemical Reviews 110 (2010) 6595–6663.
[4] B.E. Hardin, H.J. Snaith, M.D. McGehee, Nature Photonics 6 (2012) 162–169.
[5] M. Grätzel, Inorganic Chemistry 44 (2005) 6841–6851.
[6] A. Yella, H.W. Lee, H.N. Tsao, C. Yi, A.K. Chandiran, M.K. Nazeeruddin, E.W. Diau, C.Y. Yeh, S.M. Zakeeruddin, M. Gratzel, Science 334 (2011) 629–634.
[7] M. Zukalova, A. Zukal, L. Kavan, M.K. Nazeeruddin, P. Liska, M. Gratzel, Nano Letters 5 (2005) 1789–1792.
[8] A.C. Fisher, L.M. Peter, E.A. Ponomarev, A.B. Walker, K.G.U. Wijayantha, The Journal of Physical Chemistry B 104 (2000) 949–958.
[9] S. Nakade, M. Matsuda, S. Kambe, Y. Saito, T. Kitamura, T. Sakata, Y. Wada, H. Mori, S. Yanagida, The Journal of Physical Chemistry B 106 (2002) 10004–10010.
[10] T. Oekermann, D. Zhang, T. Yoshida, H. Minoura, The Journal of Physical Chemistry B 108 (2004) 2227–2235.
[11] K.D. Benkstein, N. Kopidakis, J. van de Lagemaat, A.J. Frank, The Journal of Physical Chemistry B 107 (2003) 7759–7767.
[12] J. Nelson, Physical Review B 59 (1999) 15374–15380.
[13] Q. Miao, L. Wu, J. Cui, M. Huang, T. Ma, Advanced Materials 23 (2011) 2764–2768.
[14] M. Law, L.E. Greene, J.C. Johnson, R. Saykally, P. Yang, Nature Materials 4 (2005) 455–459.
[15] S.H. Kang, S.H. Choi, M.S. Kang, J.Y. Kim, H.S. Kim, T. Hyeon, Y.E. Sung, Advanced Materials 20 (2008) 54–58.
[16] C. Rho, J.-H. Min, J.S. Suh, The Journal of Physical Chemistry C 116 (2012) 7213–7218.
[17] S.H. Kang, H.S. Kim, J.-Y. Kim, Y.-E. Sung, Nanotechnology 20 (2009) 355307–355311.
[18] P. Roy, D. Kim, K. Lee, E. Spiecker, P. Schmuki, Nanoscale 2 (2010) 45–59.
[19] M. Adachi, Y. Murata, J. Takao, J. Jiu, M. Sakamoto, F. Wang, Journal of the American Chemical Society 126 (2004) 14943–14949.
[20] J.M. Macak, H. Tsuchiya, L. Taveira, S. Aldabergerova, P. Schmuki, Angewandte Chemie International Edition 44 (2005) 7463–7465.
[21] J.R. Jennings, A. Ghicov, L.M. Peter, P. Schmuki, A.B. Walker, Journal of the American Chemical Society 130 (2008) 13364–13372.
[22] R. Mohammadpour, A. Iraji zad, A. Hagfeldt, G. Boschloo, ChemPhysChem 11 (2010) 2140–2145.
[23] J. Lin, J. Chen, X. Chen, Nanoscale Research Letters 6 (2011) 475–479.
[24] B.-X. Lei, J.-Y. Liao, R. Zhang, J. Wang, C.-Y. Su, D.-B. Kuang, The Journal of Physical Chemistry C 114 (2010) 15228–15233.
[25] G.K. Mor, O.K. Varghese, M. Paulose, C.A. Grimes, Advanced Functional Materials 15 (2005) 1291–1296.
[26] P. Charoensirithavorn, Y. Ogomi, T. Sagawa, S. Hayase, S. Yoshikawa, Journal of The Electrochemical Society 157 (2010) B354–B356.
[27] M. Ye, X. Xin, C. Lin, Z. Lin, Nano Letters 11 (2011) 3214–3220.
[28] S.Y. Ho, C. Su, C.C. Cheng, S. Kathirvel, C.Y. Li, W.R. Li, Nanoscale Research Letters 7 (2012) 147–155.
[29] D. Kim, P. Roy, K. Lee, P. Schmuki, Electrochemistry Communications 12 (2010) 574–578.
[30] B.C. O'Regan, J.R. Durrant, P.M. Sommeling, N.J. Bakker, The Journal of Physical Chemistry C 111 (2007) 14001–14010.
[31] P.M. Sommeling, B.C. O'Regan, R.R. Haswell, H.J.P. Smit, N.J. Bakker, J.J.T. Smits, J.M. Kroon, J.A.M. van Roosmalen, The Journal of Physical Chemistry B 110 (2006) 19191–19197.
[32] L. Vesce, R. Riccitelli, G. Soscia, T.M. Brown, A. Di Carlo, A. Reale, Journal of Non-Crystalline Solids 356 (2010) 1958–1961.
[33] W. Xu, S. Dai, L. Hu, C. Zhang, S. Xiao, X. Luo, W. Jing, K. Wang, Plasma Science and Technology 9 (2007) 556–559.
[34] H. Yu, S. Zhang, H. Zhao, B. Xue, P. Liu, G. Will, The Journal of Physical Chemistry C 113 (2009) 16277–16282.
[35] J. Luo, L. Gao, J. Sun, Y. Liu, RSC Advances 2 (2012) 1884–1889.
[36] W.-K. Tu, C.-J. Lin, A. Chatterjee, G.-H. Shiau, S.-H. Chien, Journal of Power Sources 203 (2012) 297–301.
[37] C.H. Lee, S.W. Rhee, H.W. Choi, Nanoscale Research Letters 7 (2012) 48–52.
[38] B.M. David, D. Qing, B. Laure, A.C. Rachel, C. Yi-Bing, P.S. George, S. Leone, Nanotechnology 18 (2007) 125608–125618.
[39] P. Roy, D. Kim, I. Paramasivam, P. Schmuki, Electrochemistry Communications 11 (2009) 1001–1004.
[40] G.D. Sharma, P. Suresh, J.A. Mikroyannidis, Electrochimica Acta 55 (2010) 2368–2372.
[41] X. Yan, D. Pan, Z. Li, Y. Liu, J. Zhang, G. Xu, M. Wu, Materials Letters 64 (2010) 1833–1835.
[42] N. Koide, A. Islam, Y. Chiba, L. Han, Journal of Photochemistry and Photobiology A: Chemistry 182 (2006) 296–305.
[43] F. Fabregat-Santiago, J. Bisquert, G. Garcia-Belmonte, G. Boschloo, A. Hagfeldt, Solar Energy Materials and Solar Cells 87 (2005) 117–131.
[44] J.-Y. Kim, K.J. Lee, S.H. Kang, J. Shin, Y.-E. Sung, The Journal of Physical Chemistry C 115 (2011) 19979–19985.
[45] K.-M. Lee, V. Suryanarayanan, J.-H. Huang, K.R.J. Thomas, J.T. Lin, K.-C. Ho, Electrochimica Acta 54 (2009) 4123–4130.
[46] G. Dai, L. Zhao, J. Li, L. Wan, F. Hu, Z. Xu, B. Dong, H. Lu, S. Wang, J. Yu, Journal of Colloid and Interface Science 365 (2012) 46–52.
[47] H. Park, W.-R. Kim, H.-T. Jeong, J.-J. Lee, H.-G. Kim, W.-Y. Choi, Solar Energy Materials and Solar Cells 95 (2011) 184–189.
[48] S. Lee, I.-S. Cho, J.H. Lee, D.H. Kim, D.W. Kim, J.Y. Kim, H. Shin, J.-K. Lee, H.S. Jung, N.-G. Park, K. Kim, M.J. Ko, K.S. Hong, Chemistry of Materials 22 (2010) 1958–1965.
[49] K. Fan, C. Gong, T. Peng, J. Chen, J. Xia, Nanoscale 3 (2011) 3900–3906.